Flow-induced vibrations of two tandem circular cylinders in a parallel-wall channel

Ren-Jie Jiang, Jian-Zhong Lin, and Xiao-Ke Ku

Citation: Physics of Fluids **26**, 104102 (2014); doi: 10.1063/1.4898341
View online: http://dx.doi.org/10.1063/1.4898341
View Table of Contents: http://scitation.aip.org/content/aip/journal/pof2/26/10?ver=pdfcov
Published by the AIP Publishing

PHYSICS OF FLUIDS **26**, 104102 (2014)

Flow-induced vibrations of two tandem circular cylinders in a parallel-wall channel

Ren-Jie Jiang,[1,2] Jian-Zhong Lin,[1,a)] and Xiao-Ke Ku[3]
[1]*The State Key Laboratory of Fluid Power Transmission and Control, Zhejiang University, Hangzhou 310027, China*
[2]*Faculty of Maritime and Transportation, Ningbo University, Ningbo 315211, China*
[3]*Department of Energy and Process Engineering, Norwegian University of Science and Technology, Norway*

(Received 4 May 2014; accepted 6 October 2014; published online 16 October 2014)

Flow-induced vibrations of one and two tandem circular cylinders in the flow around cylinders in a parallel-wall channel are numerically studied by the lattice Boltzmann method. Within a range of Reynolds number $Re = [1, 160]$, the effects of streamwise separation between two cylinders $S/D = [1.25, 3]$, mass ratio $M = [0.05, 5]$, and blockage ratio $\beta = [1/2, 1/8]$ on the motions of cylinders and fluids are investigated, respectively. For the case of an isolated cylinder, as the mass ratio is 1, no large-amplitude oscillation is observed, and as the mass ratio is 0.1, the cylinder motion translates from the steady regime to the biased periodic vibration with a large oscillation amplitude gradually as Reynolds number is increased from 1 to 160. For the case of two cylinders in tandem, two steady regimes and a variety of distinct oscillation regimes with the corresponding flow structures are observed. The critical mass ratio of the two tandem cylinders in the strong coupling regime is about an order of magnitude larger than that of an isolated cylinder. For blockage ratio is more than 1/5, the vibration type of the cylinders is exclusive, while for blockage ratio is less than 1/6, the cylinder oscillation state is bistable. The mechanisms of the observed phenomena are also discussed. © *2014 AIP Publishing LLC*. [http://dx.doi.org/10.1063/1.4898341]

I. INTRODUCTION

Flow-induced vibrations (FIV) exist extensively in our everyday life, such as the flags dancing in the wind and the plants swinging in the water.

An important type of FIV is the vortex-induced vibrations (VIV),[1,2] which has been found in many engineering applications, such as power lines, bridge piers, and off-shore engineering structures. For flow past a flexible slender body, oscillations will be excited by the interaction of the structural elasticity and the periodic hydrodynamic force induced by the shedding vortices. A significant phenomenon found in the VIV is the synchronization/lock-in. As the vortex formation frequency is close to the structural natural frequency, the body oscillation will cause the vortex shedding frequency match the oscillation frequency, and the response amplitude of the oscillator has a significant jump with a phase transition of force fluctuation and oscillator displacement. In order to facilitate to the research, such a model system is usually simplified into an elastically mounted rigid cylinder. After Feng's[3] pioneering work, a series of experimental and numerical studies about the VIV of an elastically mounted cylinder in both one degree of freedom (1-DOF, the cylinder can only move in the transverse direction) and two degrees of freedom (2-DOF, the cylinder can move in both the streamwise and transverse directions) have been performed.[3–9]

Zhou *et al.*[4] numerically studied the VIV of a circular cylinder on elastic supports and result demonstrated that a lighter cylinder usually undergoes oscillation with a larger amplitude than that of

a)Author to whom correspondence should be addressed. Electronic mail: jzlin@sfp.zju.edu.cn. Tel.: +86-571-86836009. FAX: +86-571-86914401.

a heavier one, while the structural damping will decrease the vibration amplitude. The phenomenon of critical mass ratio, below which large-amplitude oscillations are excited, for VIV of a cylinder with low structural elasticity and damping was experimentally investigated by a hydroelastic apparatus and was theoretically analyzed.[5,6] The critical mass ratio is found about 0.54 in the experimental conditions, which is in good quantitative agreement with the theoretical value. It was also inferred that the critical mass ratio of $Re = 100$ is about 0.25. Jauvtis and Williamson[7] experimentally studied the VIV of a cylinder and confirmed that the freedom to move in two directions has little effect on the transverse response and the oscillation modes. Mittal and Singh[8] numerically indicated that there exists the 2-DOF VIV of a cylinder with no structural damping at subcritical Reynolds number region ($Re_{sub} < Re_c$, and $Re_c = 47$, representing the point at where periodic flow appears for flow past a stationary circular cylinder) and synchronization occurs extensively. The mass of the oscillator plays a significant role in determining the proximity of the vortex shedding frequency to the structural natural frequency and no hysteresis was observed. Prasanth *et al.*[9] studied the effect of blockage on 2-DOF VIV at low Reynolds numbers ($Re \leq 150$). The blockage ratio is changed between 1% and 5% and it was found that the blockage effects are significant to the hysteretic behavior and the wake structure. For the case with 5% blockage, a hysteresis phenomenon close to the lower and upper limits of the synchronization were observed depending on whether the system is on the "increasing *Re*" or "decreasing *Re*" branch. The two solutions are associated with different arrangement of shedding vortices in the wake flow. While in the case of 1% blockage, the hysteretic behavior is completely eliminated.

There are a variety of arrangements for flows past a two-body system, such as tandem, side-by-side, and staggered arrangements. Previous work demonstrated that motions of the bodies and the fluids for the two-body system are more complicated than that of an isolated body. The arrangement and separation usually play significant roles. When the two bodies are placed in close proximity, the gap flow will have significant influences on the body motions.

In the flows past two elastically mounted rigid cylinders,[10–13] it has been demonstrated that the cylinder motions have complicated effects on each other.

Zdravkovich[10] investigated the VIV of two circular cylinders in various arrangements. The mechanism of VIV was found to be excited by vortex shedding or fluid-elastic. All types of the fluid-elastic oscillations were shown to be related to the regions of interference and the responses of cylinders were classified into three distinct categories. For the tandem arrangement, in most cases the amplitude of the downstream cylinder is larger than that of the upstream one, while in some cases the upstream cylinder suffers larger amplitude oscillations.

Papaioannou *et al.*[11] numerically researched the VIV of two tandem cylinders at $Re = 160$. The mass ratio is 10, the damping coefficient is 0.01, and the center-to-center spacings are 2.5, 3.5, and 5, respectively. The hysteresis effect was not observed and as the two cylinders are brought close to each other, the response curve becomes wider than that of a single cylinder. Prasanth and Mittal[12] also studied such a flow configuration with no structural damping at fixed $Re = 100$, $M = 10$, and $S/D = 5.5$. It was found that the response of the front cylinder is qualitatively similar to that of an isolated cylinder, while the rear one undergoes oscillation with larger amplitude. Synchronization and hysteresis phenomena were observed for both the cylinders. Borazjani and Sotiropoulos[13] investigated the 1- and 2-DOF VIV of two tandem cylinders in the proximity-wake interference region with $Re = 200$ and $S/D = 1.5$. Compared with the case of an isolated cylinder, oscillations of larger amplitudes and a wider lock-in region were observed in the two-cylinder system. At high reduced velocity, the two cylinders approach each other and vibrate together as a single body with vibration amplitudes up to 50% lower than that of the 1-DOF system.

Besides the VIV of a flexible body, some other types of VIV, such as flow past a tethered cylinder[14,15] and flow past a tethered sphere,[16,17] have also been studied. A variety of distinct vibration regimes with the corresponding vortex shedding modes were observed and the phenomenon of the critical mass ratio has also been studied.

Recently, a model system: the Poiseuille flow-induced vibrations (PFIV), representing the flow-induced vibrations of cylinders in a parallel-wall channel was introduced by our group.[18,19] The cylinder motions and flow structures for the cases of an isolated circular cylinder and two side-by-side and tandem cylinders were preliminarily investigated.[18,19] The PFIV model system was

mainly motivated by the phenomena of VIV and the influences of plane boundaries on flows past a stationary cylinder.[20–22] The main characteristic of the PFIV is that the distribution of the transverse hydrodynamic force on the cylinder surface affected by the channel wall plays an important role, while not the interaction of the flow and structural spring, by which the cylinder oscillations are mainly excited in the cases of flows past an elastically mounted cylinder,[1–9] a tethered cylinder[14,15] and a tethered sphere.[16,17]

In the previous work of PFIV of two tandem cylinder,[19] we focused on the effects of the streamwise separation on the cylinder motions and the corresponding flow patterns. Result shows that as the two cylinders are placed in close, the two cylinders behave as a strong coupling regime and a variety of distinct vibration regimes were observed. By comparing with the results of the cases of an isolated cylinder and two tandem cylinders with small streamwise separation, it is also noted that the critical mass ratio, beyond which the large-amplitude oscillations disappear, of the two tandem cylinders is much larger than that of an isolated one. In PFIV, besides the separation, the Reynolds number, mass ratio, and blockage ratio are some other important parameters. The present work is a further study of PFIV of two cylinders in tandem, the complicated effects of the Reynolds number, separation, mass ratio, and blockage ratio on the motions of cylinders and fluids are systematically investigated.

II. PROBLEM STATEMENT AND THE GOVERNING EQUATIONS

Figure 1 shows the schematic diagram of the flow configuration with a pair of identical circular cylinders arranged in tandem immersed into the viscous incompressible fluid between two parallel walls. The cylinders are free to move in the transverse direction under the hydrodynamic force exerted on the cylinder surface, while are fixed in the streamwise direction. The fluid is of constant density ρ and kinematic viscosity ν, and the motion of the fluid is governed by the Navier-Stokes equations. Using the inlet centerline velocity U and the cylinder diameter D, as the characteristic velocity and length, the dimensionless continuity and momentum equations can be written as follows:

$$\nabla \cdot \mathbf{u} = 0, \quad \frac{\partial \mathbf{u}}{\partial t} + \mathbf{u} \cdot \nabla \mathbf{u} = -\nabla P + \frac{1}{Re}\nabla^2 \mathbf{u}, \tag{1}$$

where $\mathbf{u}$ is the velocity vector, P is the fluid pressure, and $Re = UD/\nu$ is the Reynolds number.

The cylinder motions obey the Newton's second law:

$$\frac{d^2 Y_\alpha}{dt^2} = \frac{2C_{L\alpha}}{\pi M}, \quad \alpha = 1, 2. \tag{2}$$

where Y is the transverse displacement and the subscripts $\alpha = 1, 2$ represent the front and rear cylinders, respectively. In the above equation, the dimensionless parameters are defined as follows:

$$\text{mass ratio } M = \frac{4m}{\pi \rho D^2}, \tag{3}$$

$$\text{lift coefficient } C_{L\alpha} = \frac{2F_{y\alpha}}{\rho U^2 D}, \tag{4}$$

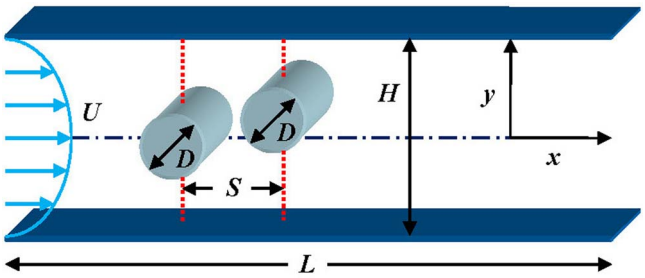

FIG. 1. Schematic diagram of flow-induced vibrations of two tandem cylinders in a parallel-wall channel.

where m is the actual mass of the cylinder and F_y is the instantaneous transverse hydrodynamic force on the cylinder surface.

The vibration Strouhal number is defined as

$$St_v = \frac{f_v D}{U}, \tag{5}$$

where f_v is the vibration frequency of the cylinder, which is always equal to vortex shedding frequency in all the present simulations.

Such a model system is mainly governed by the follow dimensionless physical parameters: the Reynolds number (Re), the mass ratio (M), the blockage ratio ($\beta = D/H$, where H is the channel width), and the streamwise separation between the two cylinders (S/D). In the present study, the effects of $Re = [1, 160]$, $S/D = [1.25, 3]$, $M = [0.05, 5]$, and $\beta = [1/2, 1/8]$ on the behaviors of cylinders and wake structures will be systematically investigated.

For the flow past a stationary cylinder, the flow structure is confirmed to be two-dimensional as Re is less than 200,[22] while in the present study Re is always less than 160, so a two-dimensional flow is adopted here.

III. LATTICE BOLTZMANN METHOD

The lattice Boltzmann method (LBM) has been developed into a promising numerical tool in computational fluid dynamics.[23] A distinct characteristic of the LBM is to obtain the macroscopic averaged properties that obey the desired macroscopic equations by constructing simplified kinetic models.

The lattice Boltzmann equation based on the BGK collision term can be written as[24–26]

$$f_i(\mathbf{x} + \mathbf{e}_i \delta t, t + \delta t) - f_i(\mathbf{x}, t) = -\frac{1}{\tau}[f_i(\mathbf{x}, t) - f_i^{eq}(\mathbf{x}, t)], \quad i = 0, 1, ..., N, \tag{6}$$

where $f_i(\mathbf{x}, t)$ is the density distribution function in the ith direction in the phase space, and $f_i^{eq}(\mathbf{x}, t)$ is the local equilibrium distribution function, δt is the time step, and τ is the relaxation time. The execution of the lattice Boltzmann equation can be separated into two steps: collision and streaming.

The two-dimensional-nine-speed model (D2Q9) is adopted in this work. As shown in Fig. 2, the velocity vector of D2Q9 is discretized into nine directions:

$$\mathbf{e}_i = \begin{cases} (0, 0), & i = 0 \\ c[\cos(i-1)\pi/2,\ \sin(i-1)\pi/2], & i = 1 \sim 4 \\ \sqrt{2}c[\cos(2i-1)\pi/4,\ \sin(2i-1)\pi/4], & i = 5 \sim 8 \end{cases}, \tag{7}$$

where $c = \delta x/\delta t$ is the lattice speed. The equilibrium distribution functions are described by

$$f_i^{eq}(\mathbf{x}, t) = \rho w_i [1 + \frac{3(\mathbf{e}_i \cdot \mathbf{u})}{c^2} + \frac{9(\mathbf{e}_i \cdot \mathbf{u})^2}{2c^4} - \frac{3u^2}{2c^2}], \tag{8}$$

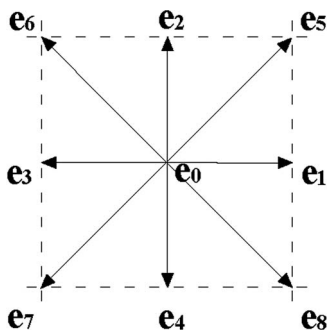

FIG. 2. Discrete velocity vector for the two-dimensional-nine-speed lattice model.

with the weight coefficients are

$$w_i = \begin{cases} 4/9, & i = 0 \\ 1/9, & i = 1 \sim 4 \\ 1/36, & i = 5 \sim 8 \end{cases}. \tag{9}$$

In such a model, the macroscopic fluid mass density ρ and momentum density $\rho\mathbf{u}$ can be obtained from

$$\rho = \sum_i f_i, \quad \rho\mathbf{u} = \sum_i f_i \mathbf{e}_i. \tag{10}$$

The fluid pressure p and kinetic viscosity ν are given by

$$p = \rho c_s^2, \quad \nu = \frac{\delta t(\tau - 0.5)c^2}{3}, \tag{11}$$

where $c_s = c/\sqrt{3}$ is the sound speed.

It has been proved that the lattice Boltzmann equation can recover the Navier-Stokes equations through the multi-scaling expansion.[27]

At the inlet boundary, a laminar parabolic velocity profile is adopted:

$$U_{\text{in}} = U[1 - (\frac{2y}{H})^2], \quad -\frac{H}{2} \le y \le \frac{H}{2}, \tag{12}$$

and at the outlet boundary, a constant pressure condition corresponding to $\rho = 1$ is applied. A no-slip boundary condition is used for the cylinder surface, upper and lower channel walls.

Several treatments have been developed for the curved solid boundary in the last decades[28–30] and the extrapolation method,[30] which has been proved to be of second order accuracy and has well-behaved stability characteristics, is chosen in the present study.

As shown in Fig. 3, a physical boundary node $\mathbf{x}_b$ is intersected between the adjacent fluid node $\mathbf{x}_f$ and solid node $\mathbf{x}_w$. The fraction of intersected link is defined as

$$q = \frac{|\mathbf{x}_f - \mathbf{x}_b|}{|\mathbf{x}_f - \mathbf{x}_w|}. \tag{13}$$

The distribution function $f_i(\mathbf{x}_f, t)$ at the node $\boldsymbol{x}_f$ is known after the collision step. However, the distribution function $f_i(\mathbf{x}_w, t)$ that moves from $\mathbf{x}_w$ to $\mathbf{x}_f$ in the streaming step is needed to know. The basic idea of the extrapolation method is to decompose the distribution at the solid node into the equilibrium part and the non-equilibrium part to get $f_i(\mathbf{x}_w, t)$, which can be expressed as

$$f_i(\mathbf{x}_w, t) = f_i^{\text{eq}}(\mathbf{x}_w, t) + f_i^{\text{neq}}(\mathbf{x}_w, t). \tag{14}$$

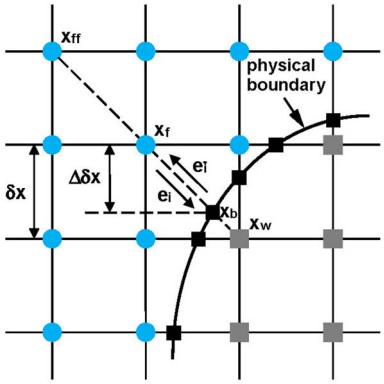

FIG. 3. The nearby fluid and solid nodes of a curved boundary.

The equilibrium part of distribution $f_i^{\mathrm{eq}}(\mathbf{x}_w, t)$ can be approximated by a fictitious one:

$$f_i^{*,\mathrm{eq}}(\mathbf{x}_w, t) = \rho w_i \left[1 + [\frac{3(\mathbf{e}_i \cdot \mathbf{u}_w)}{c^2} + \frac{9(\mathbf{e}_i \cdot \mathbf{u}_w)^2}{2c^4} - \frac{3u_w^2}{2c^2}]\right], \tag{15}$$

with the velocity at the solid node:

$$\mathbf{u}_w = \begin{cases} [\mathbf{u}_b + (q-1)\mathbf{u}_f]/q, & q \geq q_{\mathrm{c}} \\ \mathbf{u}_b + (q-1)\mathbf{u}_f + \frac{1-q}{1+q}[2\mathbf{u}_b + (q-1)\mathbf{u}_{ff}], & q < q_{\mathrm{c}} \end{cases}. \tag{16}$$

The non-equilibrium part of distribution $f_i^{\mathrm{neq}}(\mathbf{x}_w, t)$ can be extrapolated by the non-equilibrium part of distribution at the nearby fluid nodes $\mathbf{x}_f$ and $\mathbf{x}_{ff}$:

$$f_i^{\mathrm{neq}}(\mathbf{x}_w, t) = \begin{cases} f_i(\mathbf{x}_f, t) - f_i^{\mathrm{eq}}(\mathbf{x}_f, t), & q \geq q_{\mathrm{c}} \\ q[f_i(\mathbf{x}_f, t) - f_i^{\mathrm{eq}}(\mathbf{x}_f, t)] + (1-q)[f_i(\mathbf{x}_{ff}, t) - f_i^{\mathrm{eq}}(\mathbf{x}_{ff}, t)], & q < q_{\mathrm{c}} \end{cases}. \tag{17}$$

In the current study, the judgment condition $q_{\mathrm{c}} \in [0, 1]$ is $q_{\mathrm{c}} = 0.75$.

Using the LBM in combination with the extrapolation method, we can obtain the distribution functions at the fluid node $\mathbf{x}_f$ and solid node $\mathbf{x}_w$. For each relevant direction from $\mathbf{x}_f$ to $\mathbf{x}_w$, the solid boundary will obtain an amount of momentum $[f_i(\mathbf{x}_f, t)\mathbf{e}_i - f_{\bar{i}}(\mathbf{x}_w, t)\mathbf{e}_{\bar{i}}]\delta x^2/\delta t$, where $\mathbf{e}_{\bar{i}} = -\mathbf{e}_i$, as shown in Fig. 3. The two terms of the momentum represent a fraction of the fluid particle at $\mathbf{x}_f$ colliding on the boundary and a particle fraction bouncing back from $\mathbf{x}_w$ to the physical boundary, respectively. Therefore, the hydrodynamic force exerted on the boundary node is

$$F(\mathbf{x}_b) = \sum_i \frac{\delta x^2[f_i(\mathbf{x}_f, t) + f_{\bar{i}}(\mathbf{x}_w, t)]\mathbf{e}_i}{\delta t}, \tag{18}$$

then the total transverse force on the solid boundary can be obtained by

$$F_y = \sum\nolimits_{\perp} F(\mathbf{x}_b). \tag{19}$$

After the total transverse force on the cylinder surface is computed, Eq. (2) can be solved by a so called half-step "leap-frog" scheme:[31]

$$\begin{aligned} V_\alpha(t + \tfrac{1}{2}\delta t) &= V_\alpha(t - \tfrac{1}{2}\delta t) + \delta t \tfrac{2C_{L\alpha}(t)}{\pi M}, \\ Y_\alpha(t + \delta t) &= Y_\alpha(t) + \delta t V_\alpha(t + \tfrac{1}{2}\delta t), \end{aligned} \tag{20}$$

where V is the transverse velocity of the cylinder.

IV. RESULTS AND DISCUSSIONS

A. Validation of algorithm and computational details

The present algorithm is validated by applying it to the 1-DOF VIV of an elastically mounted cylinder. The physical parameters are $Re = 150$, $U_R = [3, 8]$, and $M = 2$ ($M = m/(\rho D^2)$), respectively, to be kept the same to those of Ahn and Kallinderis.[32]

The convergence of the mesh size and the computational domain has been first studied for the VIV flow configuration at $U_R = 4$. The lattice densities are $D/\delta x = 24$, 48, 60 and the uniform incoming velocities are $U/c = 0.05$, 0.1, respectively. The computational domain are $L_x \times L_y = 32D \times 16D$, $40D \times 20D$, $48D \times 24D$, and $64D \times 32D$, where L_x and L_y are the length and width of the computational domain, respectively. For each scheme, the cylinder center is fixed at $L_x/4$ downstream of the inlet boundary. The results of vibration amplitude and period from these different schemes are summarized in Table I, where T is the non-dimensional period of the cylinder oscillation. For schemes 1–4, the computational domain is fixed at $L_x \times L_y = 48D \times 24D$ and for schemes 5–7, the lattice density is fixed at $D/\delta x = 48$ and the uniform incoming velocity is fixed at $U/c = 0.1$, respectively. Result shows the present computed amplitude and period agree well with that of Ahn and Kallinderis[32] and Borazjani and Sotiropoulos,[13] and the discrepancies of the results from all the present schemes are always within 4%.

TABLE I. Amplitude and period of the VIV of an isolated cylinder at $Re = 150$ and $U_R = 4$. For Schemes 1–4, $L_x \times L_y = 48D \times 24D$ and for Schemes 5–7, $D/\delta x = 48$, $U/c = 0.1$.

	δt	A/D	T
Scheme 1 ($D/\delta x = 24$, $U/c = 0.1$)	1/240	0.592	4.534
Scheme 2 ($D/\delta x = 48$, $U/c = 0.1$)	1/480	0.580	4.591
Scheme 3 ($D/\delta x = 60$, $U/c = 0.1$)	1/600	0.577	4.598
Scheme 4 ($D/\delta x = 60$, $U/c = 0.05$)	1/1200	0.574	4.577
Scheme 5 ($L_x \times L_y = 32D \times 16D$)	1/480	0.578	4.514
Scheme 6 ($L_x \times L_y = 40D \times 20D$)	1/480	0.577	4.570
Scheme 7 ($L_x \times L_y = 64D \times 32D$)	1/480	0.579	4.643
Ahn and Kallinderis[32]	...	0.544–0.691	4.297–4.390
Borazjani and Sotiropoulos[13]	...	0.53	...

The VIV of an elastically mounted cylinder at a reduced velocity range of $U_R = [3, 8]$ is then simulated with $D/\delta x = 48$, $U/c = 0.1$, and $L_x \times L_y = 48D \times 24D$, respectively. Figure 4 shows the response curve of the maximum vibration amplitude $A_{\max}/D$ of the cylinder as a function of U_R. As a comparison, the results of Ahn and Kallinderis[32] and Borazjani and Sotiropoulos[13] are also given. It can be seen that the previous and present results are in good quantitative agreement with each other. For $U_R = 3$, the cylinder vibrates around the equilibrium position at a small amplitude less than 0.1. As U_R is increased from 3 to 4, there is a sudden jump of $A_{\max}/D$, which corresponds to a wide vortex street, see the inset of the left image in Fig. 4. The cylinder vibrates at a large amplitude for $U_R = [4, 7]$ and the amplitude decreases slowly as U_R increases. When U_R is continually increased to 8, there is a sudden decrease of $A_{\max}/D$, corresponding to a narrow vortex street, see the inset of the right image in Fig. 4.

In this work, the blockage ratio is always changed between 1/2 and 1/8, which corresponds to a smaller computational domain than that of the unconfined case, so the scheme with $D/\delta x = 60$, $U/c = 0.05$, and $L_x = 60D$ with the cylinder center is fixed at $20D$ downstream of the inlet boundary, is adopted in the following simulations. Such a computed region is large enough and the cylinder is sufficiently far away from the inlet and outlet boundaries to eliminate the effects of the computational boundaries.

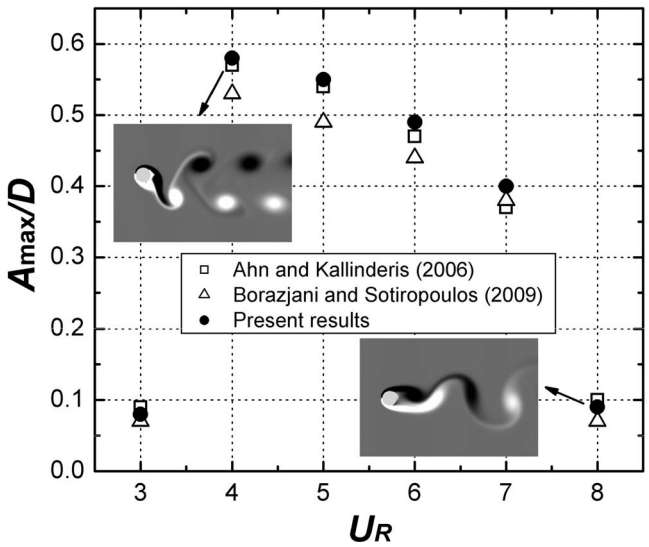

FIG. 4. The maximum vibration amplitude versus reduced velocity for vortex-induced vibration of an elastically mounted cylinder. The insets are the instantaneous wake structures for $U_R = 4$ and $U_R = 8$, respectively.

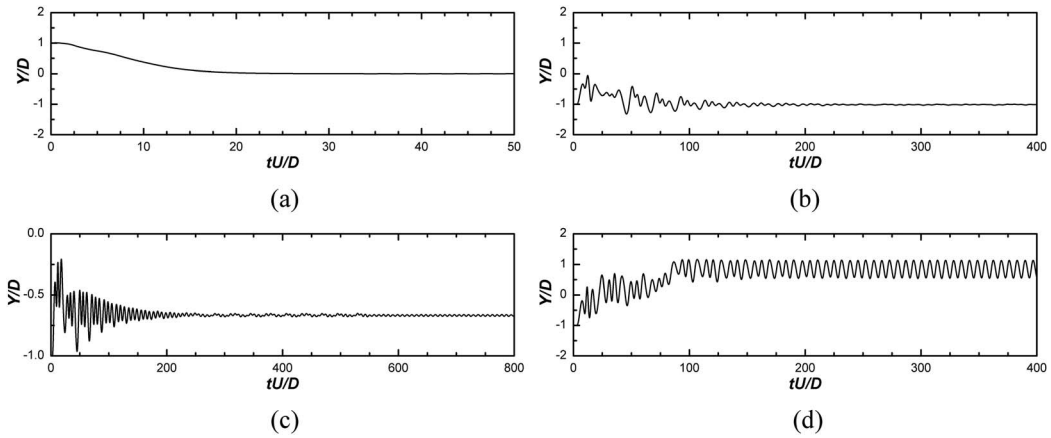

FIG. 5. Time series of transverse displacements for the flow-induced vibrations of an isolated cylinder in a parallel-wall channel with $\beta = 1/4$. (a) $Re = 1$, $M = 1$, (b) $Re = 160$, $M = 1$, (c) $Re = 60$, $M = 0.1$, and (d) $Re = 160$, $M = 0.1$.

B. Flow-induced vibrations of an isolated cylinder in a parallel-wall channel

To have a better understanding for the flow-induced vibrations of the two tandem cylinders, we first investigate the case of an isolated cylinder with the same fluid conditions and structural characteristics to that of the two-cylinder system. The blockage is fixed at $\beta = 1/4$, the mass ratio is $M = 1$ and $M = 0.1$ and the Reynolds number is in a range of $Re = [1, 160]$. For $M = 1$, no large-amplitude oscillation occurs as Re is increased from 1 to 160. For Re is changed between 1 and 30, the cylinder finally rests at the centerline of the channel, as shown in Fig. 5(a). For Re is increased from 40 to 160, the cylinder deviates from the centerline to either side of the channel and a non-periodic oscillation with the peak-to-peak vibration amplitude A/D always less than 0.02 occurs gradually, as shown in Fig. 5(b). For $M = 0.1$, when Re is between 1 and 30, the cylinder also rests at the channel centerline, just like the case of $M = 1$. For Re is changed from 40 to 60, the cylinder deviates from the centerline of the channel and a quasi-periodic oscillation with A/D less than 0.02 is observed, as shown in Fig. 5(c). For Re is increased from 70 to 160, the cylinder oscillates periodically with a considerable amplitude, as shown in Fig. 5(d). In the steady and the non-periodic small-amplitude oscillation regimes, no obvious vortex is shed in the wake of the cylinder, while in the biased periodic oscillation regime, per vortex shed in a vibration cycle comprises a single row of same-sign vortices, see Fig. 6. Figure 7 shows the relative equilibrium position σ/H, peak-to-peak vibration amplitude A/D and vibration Strouhal number St_v as functions of Reynolds number Re. Results show that as Re increases, σ/H of the cases of both $M = 1$ and $M = 0.1$ increases and σ/H of $M = 0.1$ is always less than that of $M = 1$, due to the large-amplitude oscillation of the cylinder. For Re is less than 60, no significant vibration is observed for both $M = 1$ and $M = 0.1$, and for Re is between 60 and 80, there is a sudden increase of A/D for the case of $M = 0.1$ and as Re is increased continually till to 160, both A/D and St_v of the cylinder increase monotonously.

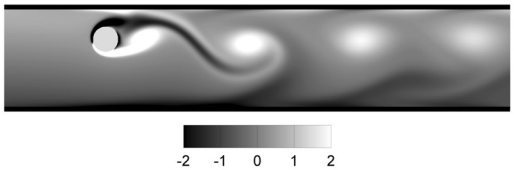

FIG. 6. Instantaneous vorticity contours for flow-induced vibrations of an isolated cylinder at $Re = 160$, $\beta = 1/4$, and $M = 0.1$.

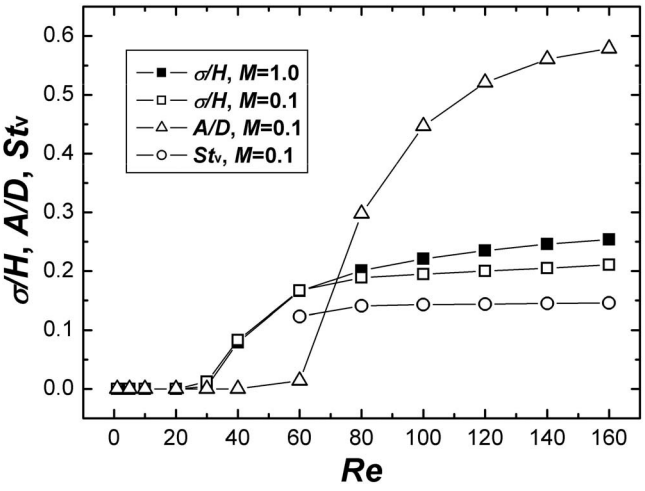

FIG. 7. Vibration parameters versus Reynolds number for the flow-induced vibrations of an isolated cylinder in a parallel-wall channel with $\beta = 1/4$.

C. Flow-induced vibrations of two tandem cylinders in a parallel-wall channel

In Secs. IV C 1–IV C 3, the flow-induced vibrations of two tandem cylinders in a plane channel in the ranges of $Re = [1, 160]$, $S/D = [1.25, 3]$, $M = [0.05, 5]$, and $\beta = [1/2, 1/8]$ are investigated, respectively. The main purpose of this work is to study the effects of the Reynolds number, separation, mass ratio, and blockage ratio on the motions of cylinders and fluids. The phenomena of critical mass ratio and critical blockage ratio are also discussed.

1. Effects of Reynolds number and streamwise separation on the flow-induced vibrations of two tandem cylinders

For our previous work, results show that when the two cylinders are placed close to each other, the cylinder motions behave as a strong coupling regime.[19] In this section, with a fixed blockage ratio of 1/4, we investigate the effect of $Re = [1, 160]$ on the behaviors of the cylinders and wake structures systematically for $M = 1$ and $M = 0.1$ and $S/D = 1.25, 1.5, 2, 3$.

Figure 8 shows the phase diagram of vibration regions in the S/D-Re plane for flow-induced vibrations of two tandem cylinders at $M = 1$ and $M = 0.1$, respectively. Result shows that for both mass ratios, when the Reynolds number is low, both cylinders behave as a steady regime. Figure 9 shows the time series of transverse displacements of the two tandem cylinders with $Re = 1$, $M = 1$, and $S/D = 1.5$. It should be noted that before the two cylinders rest at the channel centerline, there are several large oscillation cycles, while for the case of an isolated cylinder with $Re = 1$, the cylinder closes to the centerline of the channel directly, see Fig. 5(a). For $S/D = 1.25, 1.5$, besides the symmetric steady regime, another biased steady regime, representing the cylinders rest at their equilibrium positions not at the centerline of the channel, has also been observed. The biased degree, which is defined as the distance between the equilibrium position and the channel centerline, for each cylinder at $M = 1$ and $M = 0.1$ is always the same. For the separation is more than 2, such a biased steady regime has never been observed for all the present simulations. For example, Figures 10 and 11 show the time series of cylinder transverse displacements, instantaneous vorticity, and pressure contours for $Re = 10$, $M = 1$, and $S/D = 1.5, 2$, respectively.

When the Reynolds number is increased to a critical value, the cylinders oscillate at distinct regimes. For each mass ratio and separation, the critical Reynolds number is always between 20 and 40, which is in the subcritical region. The phenomenon of vortex-induced vibration and periodic vortex shedding at subcritical region has also been observed in the flows past an elastically mounted cylinder.[8] Based on the cylinder motion type, the response of cylinders can be classified into several regimes: the periodic vibration, period-doubling vibration, and quasi-periodic vibration

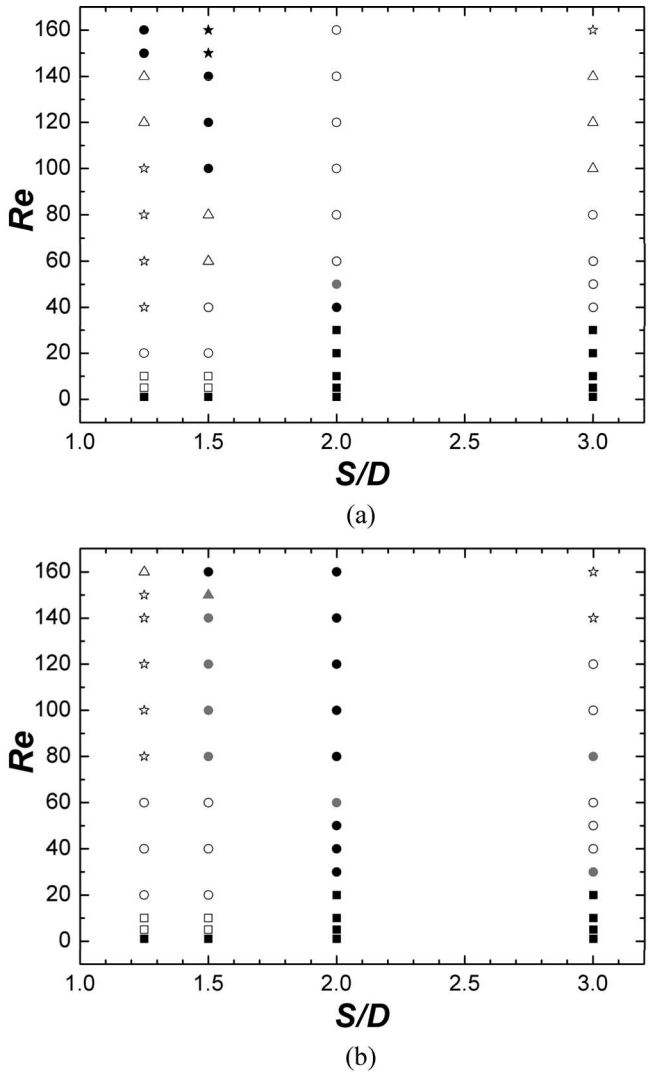

FIG. 8. Phase diagram of vibration regions in the *S*/*D*-*Re* plane for flow-induced vibrations of two tandem cylinders. The square, circle, triangle, and star represent the steady, periodic vibration, quasi-periodic vibration, and period-doubling vibration regimes, respectively. In the vibration regime, the black, gray, and hollow symbols represent the symmetric, approximately symmetric, and biased states, respectively. (a) $M = 1$ and (a) $M = 0.1$.

regimes. While based on the equilibrium position (for the vibration regime, the equilibrium position represents the oscillation axis of the cylinder), the cylinder motion can be classified into the symmetric, approximately symmetric, and biased states. For the symmetric and approximately symmetric large-amplitude oscillation regimes, two vortices shed per cycle comprise two rows of alternately rotating vortices. For the biased states in all the present simulations, the oscillation axes of both

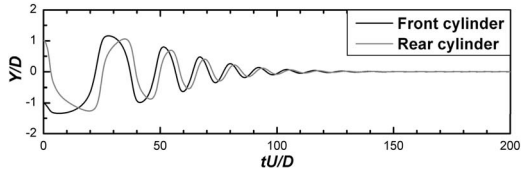

FIG. 9. Time series of transverse displacements for the flow-induced vibrations of two tandem cylinders in a parallel-wall channel with Re = 1, $\beta = 1/4$, M = 1, and S/D = 1.5.

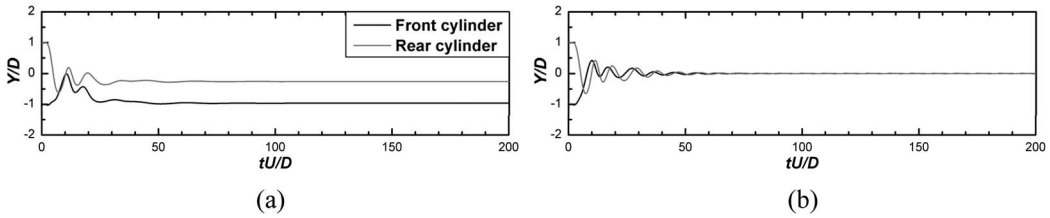

FIG. 10. Time series of transverse displacements for the flow-induced vibrations of two tandem cylinders in a parallel-wall channel with $Re = 10$, $\beta = 1/4$, and $M = 1$. (a) $S/D = 1.5$ and (a) $S/D = 2$.

cylinders are always at the same side of the channel and in the large-amplitude oscillation regimes, only a single row of vortices generates in the wake. Figures 12 and 13 show the time series of cylinder transverse displacements and instantaneous flow structures for the flow-induced vibrations of two tandem cylinders in a parallel-wall channel with $Re = 100$, 160, $M = 0.1$, $S/D = 1.25$ and $Re = 160$, $M = 1$, $S/D = 1.25$, 2, representing the biased period-doubling vibration, biased quasi-periodic vibration, symmetrical periodic vibration, and biased periodic vibration regimes, respectively.

As shown in Fig. 8(a), for $M = 1$, $S/D = 1.25$, $Re = 20$, both the cylinders behave as biased periodic vibrations. For $Re = [40, 100]$, the cylinders behave as period-doubling vibrations and the number of the subcycles increases as Re is increased. When $Re = 120$, 140 and $Re = 150$, 160, the cylinders behave as the biased quasi-periodic vibrations and symmetrical periodic vibrations, respectively. For $S/D = 1.5$, $Re = [20, 40]$ and $Re = [60, 80]$, the cylinders behave as biased periodic vibrations and biased quasi-periodic vibrations, respectively. For $Re = [100, 140]$, the cylinders translate to symmetrical periodic vibrations and for Re is more than 150, the cylinders behave as period-doubling vibrations around the centerline of the channel. For $S/D = 2$, $Re = [40, 160]$, the cylinders always oscillate periodically and as Re is more than 60, the cylinder oscillations significantly deviate from the centerline of the channel. For $S/D = 3$, the behaviors of the cylinders are very complicated. For $Re = [40, 80]$, $Re = [100, 140]$, and $Re = 160$, the cylinders behave as biased periodic vibrations, biased quasi-periodic vibrations, and biased period-doubling vibrations, respectively. Based on the above discussion, for S/D is more than 2, the equilibrium position of each cylinder close to either channel wall more and more significant as Re increases. While for S/D is

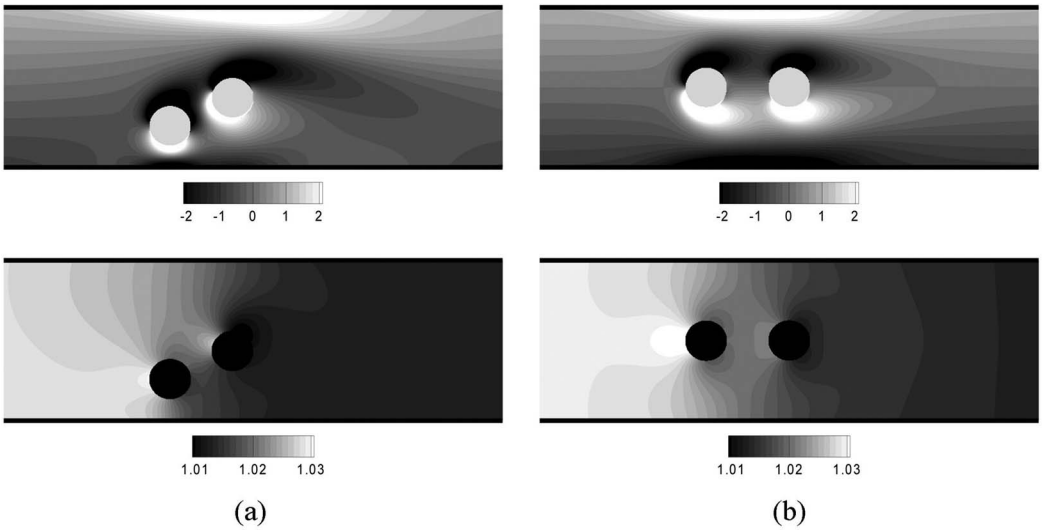

FIG. 11. Instantaneous vorticity (upper) and pressure contours (lower) for the flow-induced vibrations of two tandem cylinders in a parallel-wall channel with $Re = 10$, $\beta = 1/4$, and $M = 1$. (a) $S/D = 1.5$ and (b) $S/D = 2$.

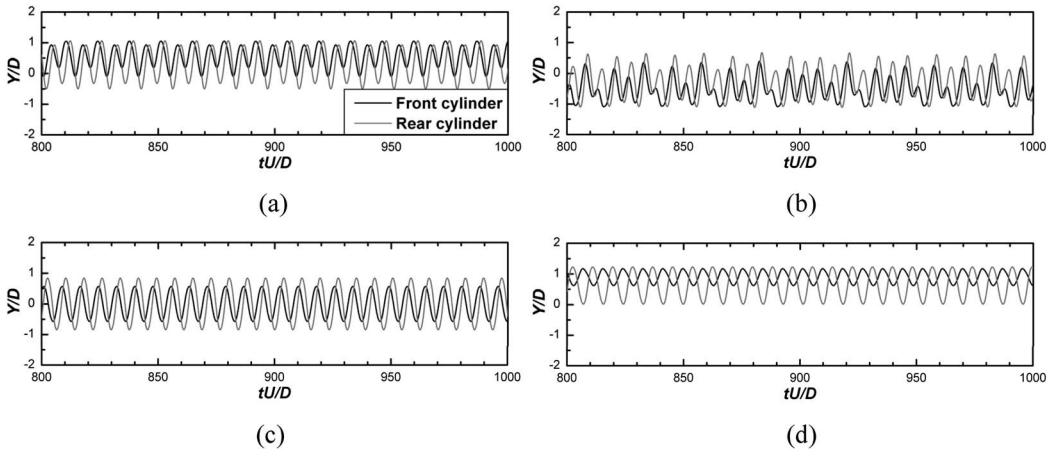

FIG. 12. Time series of transverse displacements for the flow-induced vibrations of two tandem cylinders in a parallel-wall channel with $\beta = 1/4$. (a) $Re = 100$, $M = 0.1$, $S/D = 1.25$; (b) $Re = 160$, $M = 0.1$, $S/D = 1.25$; (c) $Re = 160$, $M = 1$, $S/D = 1.25$; and (d) $Re = 160$, $M = 1$, $S/D = 2$.

less than 1.5, the equilibrium position of the cylinders close to the channel centerline gradually in the oscillation regime.

Then we continue to investigate the cylinder motions in the vibration regime with $M = 0.1$. As shown in Fig. 8(b), for $M = 0.1$, $S/D = 1.25$, $Re = [20, 60]$, both the cylinders behave as biased periodic vibrations. For $Re = [80, 150]$, the cylinders behave as period-doubling vibrations and the subcycle number increases as the Re is increased. For $Re = 160$, the cylinders behave as quasi-periodic vibrations. Figure 14 shows the power spectrum density (PSD) of cylinder transverse displacements at different Reynolds numbers. For $Re = 60$, there is only a single peak is formed in the map of PSD for each cylinder and the peaks of both cylinders appear at the same St_v, as shown in Fig. 14(a). For $Re = 100$, besides the main peak, another weaker peak with lower St_v also appears in the map of PSD for each cylinder, as shown in Fig. 14(b). As Re is increased continually, the secondary peak of PSD becomes stronger and stronger and some other frequencies also grow up, as shown in Fig. 14(c). For $Re = 160$, the tips of the main peaks become blunt, which represents the appearance of the quasi-periodic vibrations of the cylinders, as shown in Fig. 14(d). For $S/D = 1.5$, $Re = [20, 60]$, the cylinders also behave as biased periodic vibrations and for $Re = [80, 140]$, the cylinders oscillate periodically with their equilibrium positions close to the channel centerline. For $Re = 150$ and $Re = 160$ the cylinders behave as the quasi-periodic vibrations with their equilibrium

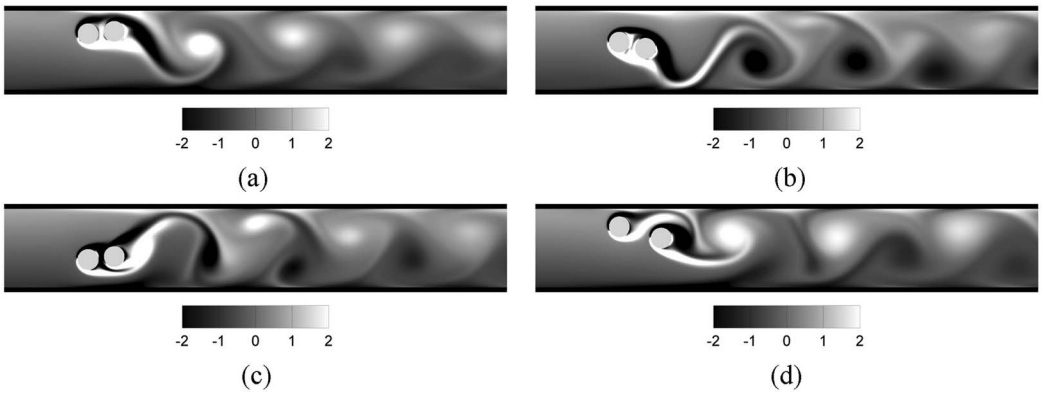

FIG. 13. Instantaneous vorticity contours for the flow-induced vibrations of two tandem cylinders in a parallel-wall channel with $\beta = 1/4$. (a) $Re = 100$, $M = 0.1$, $S/D = 1.25$; (b) $Re = 160$, $M = 0.1$, $S/D = 1.25$; (c) $Re = 160$, $M = 1$, $S/D = 1.25$; and (d) $Re = 160$, $M = 1$, $S/D = 2$.

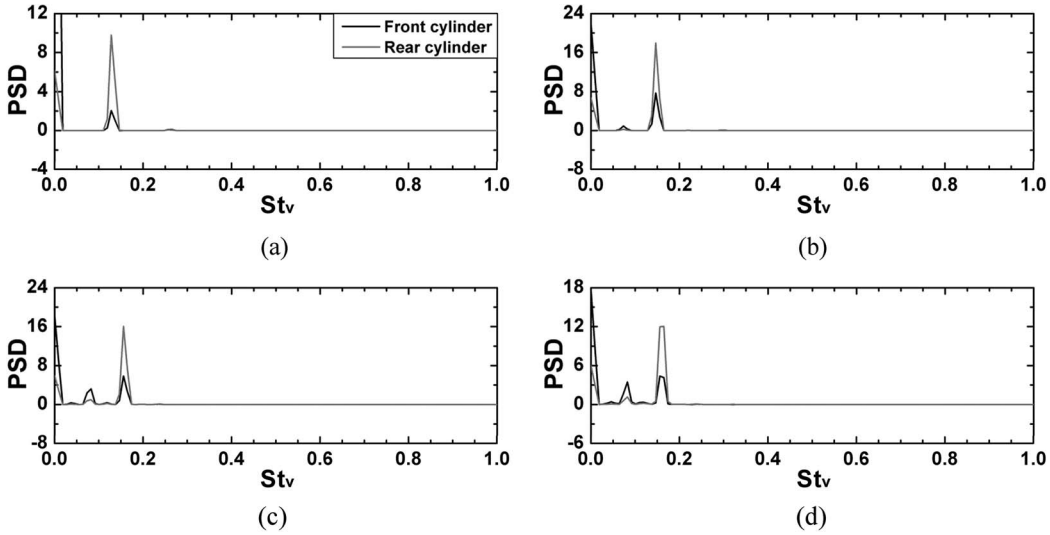

FIG. 14. Power spectrum density of cylinder displacements at different Reynolds numbers with $\beta = 1/4$, $M = 0.1$, and $S/D = 1.25$. (a) $Re = 60$, (b) $Re = 100$, (a) $Re = 140$, and (a) $Re = 160$.

positions close to the channel centerline and the symmetrical periodic vibrations, respectively. For $S/D = 2$, $Re = [30, 160]$, the cylinders always behave as the periodic vibrations, and for most situations, the cylinders oscillate symmetrically around the centerline of the channel but for $Re = 60$, the cylinder oscillation axes deviate slightly from the channel centerline. For $S/D = 3$, as Re is increased, the cylinder motions become more and more irregular and for each cylinder, the biased degree increases broadly with increasing Re. For $Re = 30$, the cylinders oscillate at small amplitudes around their equilibrium positions close to the centerline of the plane channel. For $Re = [40, 120]$, the cylinders always behave as the biased periodic vibrations, and for $Re = [140, 160]$, the cylinders behave as the period-doubling vibrations.

Based on the above discussion, for both $M = 1$ and $M = 0.1$, the behaviors of the cylinders are very complicated by comparing with the case of an isolated cylinder. For $S/D = 1.5$ and $S/D = 2$, the strong couple vibrations with large oscillation amplitudes and high oscillation frequencies, exist extensively. Figure 15 shows the relationships of peak-to-peak vibration amplitude A/D, relative equilibrium position σ/H, vibration Strouhal number St_v, phase angle $\Delta\theta$ and Reynolds number Re at $M = 1$ and $M = 0.1$ and $S/D = 1.5$ and $S/D = 2$, respectively. The phase angle is defined as

$$\Delta\theta = 2\pi \times \frac{t_{RP} - t_{FP}}{T}, \tag{21}$$

where T is the oscillation period, t_{RP} and t_{FP} represent the times at the peaks of two adjacent cycles for the front and rear cylinders, respectively.

As shown in Fig. 15(a), in the vibration regime, for both $S/D = 1.5$ and $S/D = 2$, A/D of the rear cylinder is always larger than that of the front cylinder. For $S/D = 1.5$, there are sudden jumps of A/D at $Re = [80, 100]$ for $M = 1$ and $Re = [150, 160]$ for $M = 0.1$, respectively. For $S/D = 2$, at the beginning of the response branches, A/D of each cylinder increases rapidly, and then A/D increases slowly with increasing Re. Even for $M = 1$, A/D of both cylinders are almost keep constant as Re is changed between 60 and 160.

As shown in Fig. 15(b), in the biased oscillation regime, for both $S/D = 1.5$ and $S/D = 2$, the biased degree of the front cylinder is always larger than that of the rear one. For $S/D = 1.5$, in the steady regime, as Re is increased, the relative equilibrium position σ/H increases rapidly to form a peak at $Re = 10$ for each cylinder and the values of σ/H for both cylinders with $M = 1$ and $M = 0.1$ are always the same. When the cylinder oscillations are excited, the values of σ/H for both $M = 1$ and $M = 0.1$ decrease slowly and for Re is more than 100, both the cylinders oscillate around (or near) the centerline of the channel. For $S/D = 2$ and $M = 1$, the oscillation axes of both cylinders

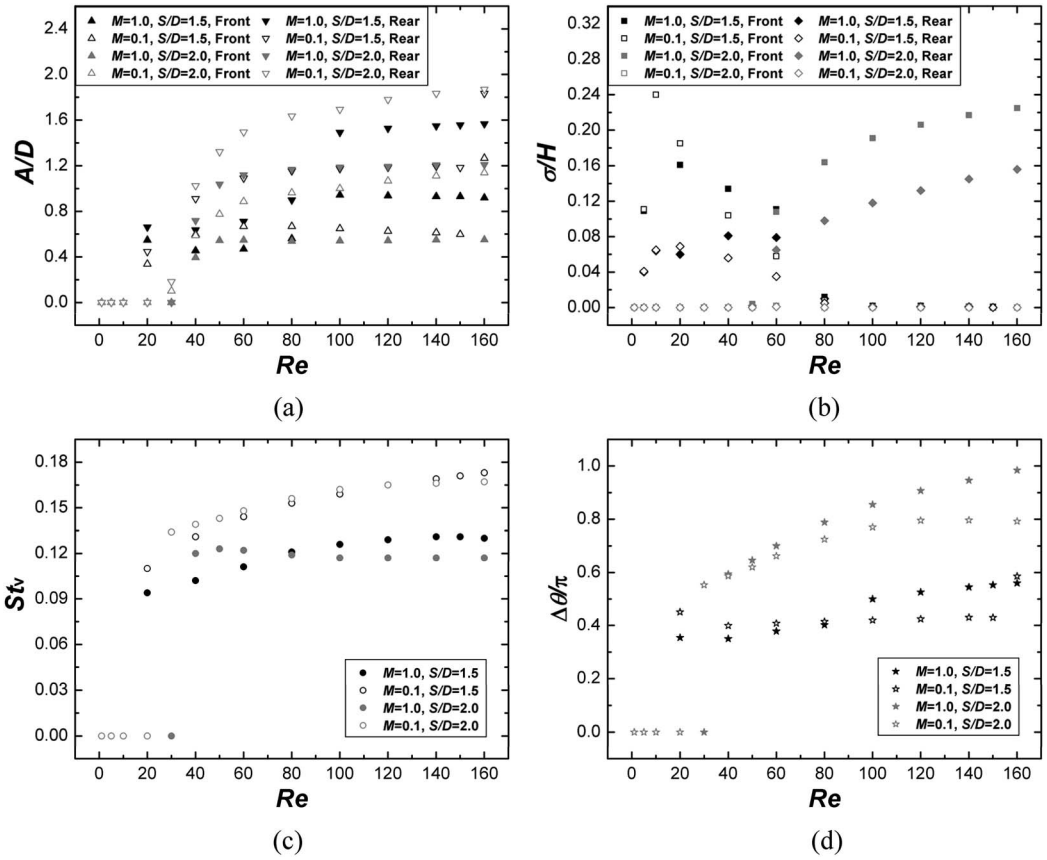

FIG. 15. Vibration parameters versus Reynolds number for the flow-induced vibrations of two tandem cylinders in a parallel-wall channel with $\beta = 1/4$. (a) Vibration amplitude, (b) relative equilibrium position, (c) vibration Strouhal number, and (d) phase angle.

deviate from the channel centerline at $Re = 50$ and σ/H of both cylinders increase with increasing Re. For $S/D = 2$ and $M = 0.1$, as Re is changed at the current range, the oscillation axes of both cylinders are always at (or near) the centerline of the channel.

As shown in Fig. 15(c), in the vibration regime, for both $S/D = 1.5$ and $S/D = 2$, St_v of $M = 0.1$ is always larger than that of $M = 1$. For $S/D = 1.5$ and $M = 1$ and $M = 0.1$, the coupled St_v increases monotonously with increasing Re. For most cases of $S/D = 2$ and $M = 1$, the coupled St_v decreases slowly as Re is increased, while for $M = 0.1$, the coupled St_v increases with increasing Re.

As shown in Fig. 15(d), in the oscillation regime, for most cases of $S/D = 1.5$ and $S/D = 2$, $\Delta\theta$ increases with increasing Re. For both $M = 1$ and $M = 0.1$, $\Delta\theta$ of $S/D = 1.5$ is always less than that of $S/D = 2$. For $S/D = 1.5$, $\Delta\theta$ of $M = 1$ is larger than that of $M = 0.1$ as Re is between 100 and 150, while is smaller than that of $M = 0.1$ at other Re. For $S/D = 2$, $\Delta\theta$ of $M = 1$ is always larger than that of $M = 0.1$ in the oscillation regime.

2. Effects of mass ratio on the flow-induced vibrations of two tandem cylinders

The mass ratio of the oscillator to the fluid also plays an important role in such a PFIV model system. In our previous study,[18] result shows that there is a critical mass ratio M_c in PFIV and at moderate Reynolds numbers, M_c of a single cylinder is usually less than 0.4 at $Re = 100$. In the present study, it is found that for the case of two cylinders in tandem, large-amplitude oscillations of both cylinders occur extensively at $M = 1$, which hints that the gap flows between the two cylinders produce a strong force on both cylinders. Based on these observed phenomena, it is necessary to investigate M_c for the case of two tandem cylinders. In this section, the effects of the mass ratio M

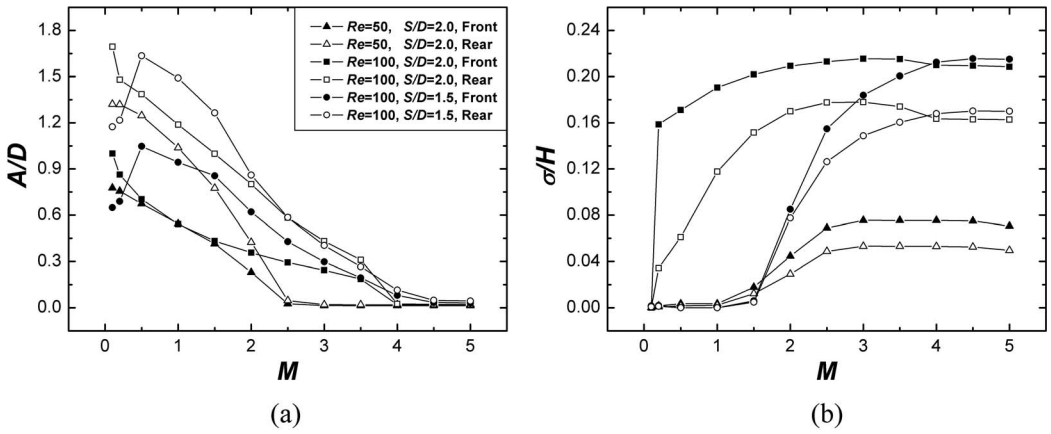

FIG. 16. Vibration parameters versus mass ratio for the flow-induced vibrations of two tandem cylinders in a parallel-wall channel with $\beta = 1/4$. (a) Vibration amplitude and (b) relative equilibrium position.

$= [0.05, 5]$ on the cylinder motions at $\beta = 1/4$, $S/D = 2$, $Re = 50$, 100 and $S/D = 1.5$, $Re = 100$ are systematically investigated with special attention to the phenomenon of critical mass ratio.

Figure 16 shows the computed vibration amplitude and relative equilibrium position versus mass ratio. In the oscillation regimes, A/D of the rear cylinder is always larger than that of the front one, while σ/H of the rear cylinder is always less than that of the front one. For $S/D = 2$ and $Re =$ 50, 100, A/D of each cylinder decreases monotonously till to zero as M is increased, and for most cases σ/H of each cylinder increases as M is increased. The critical mass ratio M_c, below which the cylinders undergo large-amplitude oscillations, of $Re = 50$ and $Re = 100$ are 2.5 and 4, respectively. For $S/D = 1.5$ and $Re = 100$, as M is increased from 0.05 to 5, A/D of each cylinder first increases and then decreases to form a peak at $M = 0.5$ and M_c is about 4. For $M \leq 1$, both cylinders oscillate around (or near) the centerline of the channel, while M is increased from 1.5, both the cylinders behave as biased oscillations and the oscillation axes move far and far away from the centerline of the channel.

3. Effects of blockage ratio on the flow-induced vibrations of two tandem cylinders

In the current model system, besides the Reynolds number, streamwise separation and mass ratio, the blockage ratio is another important parameter. In this section, the effects of the blockage ratio $\beta = [1/2, 1/8]$ on the cylinder motions and flow structures with $Re = 100$, $M = 1$, 0.1 and S/D $= 1.5$, 2 are investigated.

Numerical results show that for each mass ratio and separation, as β is changed between 1/2 and 1/5, the vibration regime is always exclusive and in such a regime, the rear cylinder is immersed into the wake of the front cylinder and both the cylinders have strong interactions with each other. As β is changed between 1/6 and 1/8, the cylinder motion is bistable. Besides the strong coupled vibration regime (Regime I), another separated vibration regime (Regime II) has also been observed. In Regime II, one cylinder move around its oscillation axis close to either channel wall, while the other cylinder oscillate around its vibration axis at the opposite side of the channel. For each case in this section, the computation is performed at least three times by placing the cylinders at different initial positions, even for $\beta = [1/4, 1/8]$, the simulation is performed at least eight times. It should be noted that in the bistable regime, the smaller the blockage ratio is, the easier the Regime II is to produce. Figures 17 and 18 show the time series of transverse displacements and flow structures for $Re = 100$, $\beta = 1/6$ and $S/D = 1.5$. Figures 17(a), 17(c), 18(a), and 18(c) and 17(b), 17(d), 18(b), and 18(d) show the results of the vibration Regimes I and II, respectively. As shown in Figs. 17(a) and 18(a), for $M = 1$, when the cylinders oscillate steadily in Regime I, both cylinders vibrate periodically with large amplitudes around the centerline of the channel, and in the wake of the rear cylinder, two alternately rotating vortices shed per oscillation cycle comprise two rows of vortices. While in Regime II, see Figs. 17(b) and 18(b), the cylinders move apart from the centerline

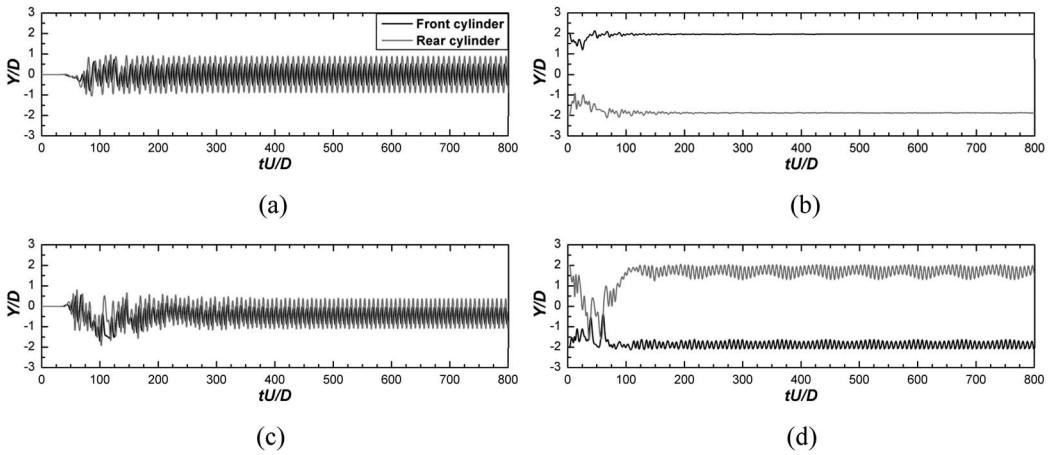

FIG. 17. Time series of transverse displacements for the flow-induced vibrations of two tandem cylinders in a parallel-wall channel with $Re = 100$, $\beta = 1/6$ and $S/D = 1.5$. (a) $M = 1$, Regime I; (b) $M = 1$, Regime II; (c) $M = 0.1$, Regime I; and (d) $M = 0.1$, Regime II.

of the channel with negligible amplitudes and in the wake of each cylinder, only a nearly stationary vortex is formed. As shown in Figs. 17(c) and 18(c), for $M = 0.1$, when the cylinders oscillate steadily in Regime I, both cylinders undergo periodic large-amplitude oscillations with their vibration axes near the channel centerline, and two alternately rotating vortices with one stronger and the other weaker generate in the wake of the rear cylinder. While in Regime II, see Figs. 17(d) and 18(d), the cylinders behave as period-doubling oscillations with their vibration axes at the opposite sides of the channel centerline and in the wake, one vortex shed from each cylinder per cycle comprises two rows of vortices.

As we have mentioned above, for the case of an isolated cylinder, for $M = 1$, no significant oscillation has been observed, while for $M = 0.1$, the cylinder vibrates periodically at a large amplitude. When in Regime II for $M = 1$, the cylinders are kept far away from each other, the rear cylinder is outside of the wake of the front cylinder and the interaction of the two cylinders is very weak, so both cylinders oscillate non-periodically with negligible amplitudes, just like two isolated ones. For $M = 0.1$ in Regime II, although the cylinders are kept apart from each other, the

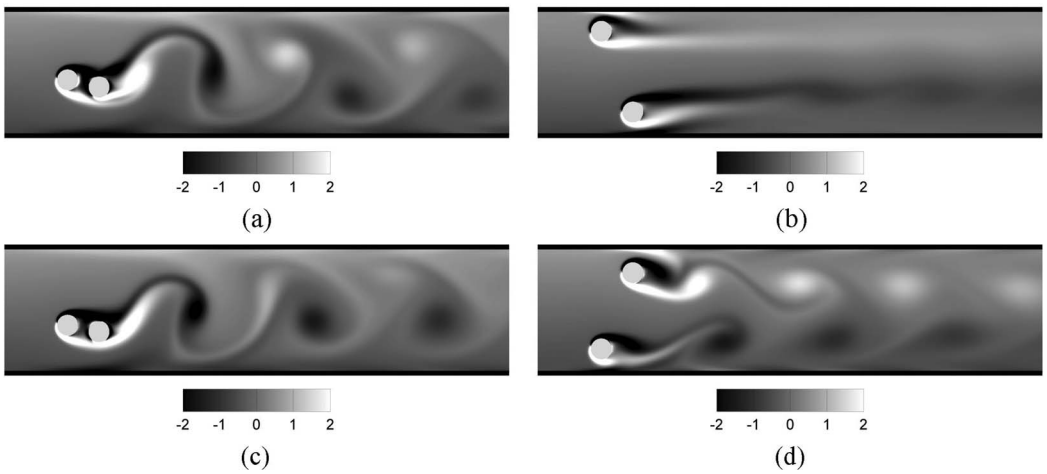

FIG. 18. Instantaneous vorticity contours for the flow-induced vibrations of two tandem cylinders in a parallel-wall channel with $Re = 100$, $\beta = 1/6$ and $S/D = 1.5$. (a) $M = 1$, Regime I; (b) $M = 1$, Regime II; (c) $M = 0.1$, Regime I; and (d) $M = 0.1$, Regime II.

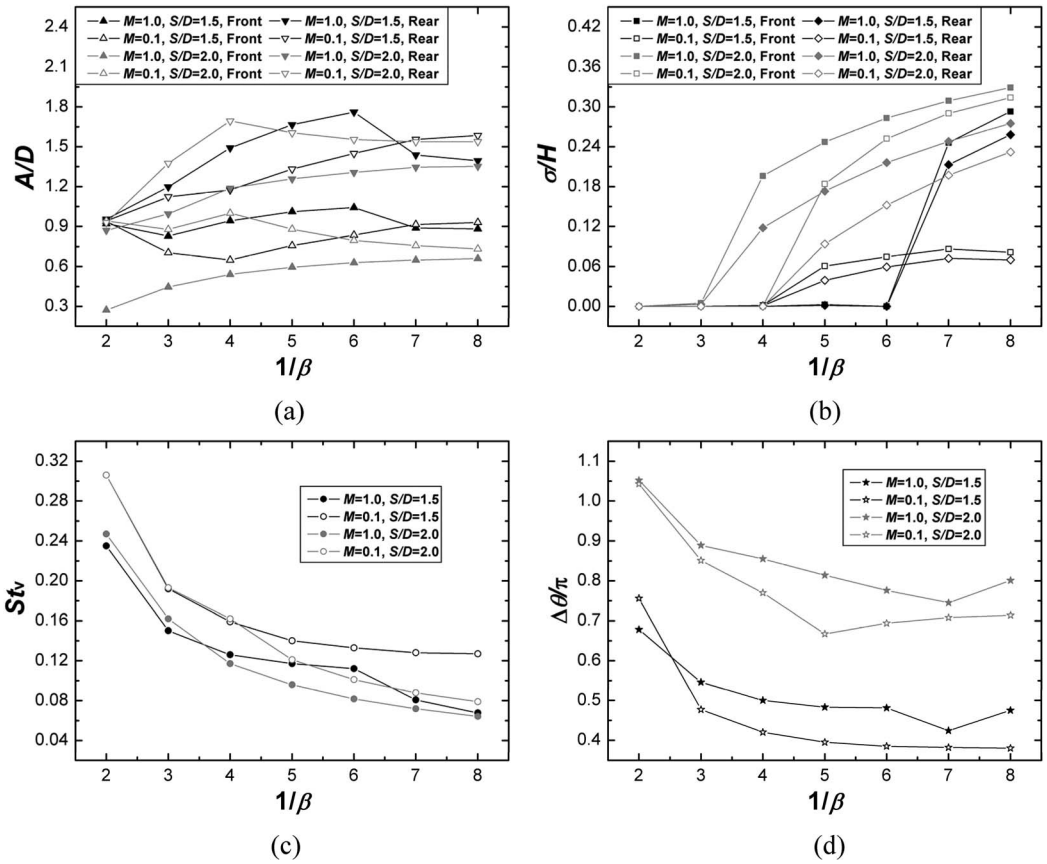

FIG. 19. Vibration parameters versus blockage ratio for the flow-induced vibrations of two tandem cylinders in a parallel-wall channel with $Re = 100$. (a) Vibration amplitude, (b) relative equilibrium position, (c) vibration Strouhal number, and (d) phase angle.

large-amplitude oscillation of each cylinder still has a significant interaction to the other one, which brings about the large-amplitude period-doubling vibrations of cylinders.

Figure 19 shows the relationships of vibration amplitude, relative equilibrium position, vibration Strouhal number, phase angle, and blockage ratio at $Re = 100$, $M = 1$ and $M = 0.1$ and $S/D = 1.5$ and $S/D = 2$, respectively. The results given in Fig. 19 are all from the vibration Regime I and in the present simulations of Regime I, the cylinders are all behave as periodic vibrations.

As shown in Fig. 19(a), in the vibration regime, for all the present simulations, A/D of the rear cylinder is always larger than that of the front one. For $S/D = 1.5$ and $M = 1$, in most cases as β is more than 1/6, A/D of both cylinders increase as β decreases and as β is between 1/6 and 1/7, there are sudden decrease of A/D for both cylinders. For $S/D = 1.5$ and $M = 0.1$, A/D of the front cylinder first decreases and then increases, while A/D of the rear cylinder increases with decreasing β. For $S/D = 2$ and $M = 1$, as β decreases, A/D of both cylinders increase monotonously, while for $M = 0.1$, A/D of each cylinder mainly first increases and then decreases to form a peak at $\beta = 1/4$.

As shown in Fig. 19(b), for all the present simulations, as β decreases, σ/H of both cylinders first at (or near) the centerline of the plane channel, and when β is decreased to a critical value, there are sudden jumps of σ/H for both cylinders. The blockage ratios at where the cylinder motions translate to the biased regime for $S/D = 1.5$ and $M = 1$, $S/D = 1.5$ and $M = 0.1$, $S/D = 2$ and $M = 1$ and $S/D = 2$ and $M = 0.1$ are 1/6, 1/4, 1/3 and 1/4, respectively. In the biased vibration regime, the biased degree of the front cylinder is always more than that of the rear one.

As shown in Fig. 19(c), for each mass ratio and separation, St_v always decreases monotonously with decreasing β and for both $S/D = 1.5$ and $S/D = 2$, St_v of $M = 0.1$ is always larger than that of $M = 1$.

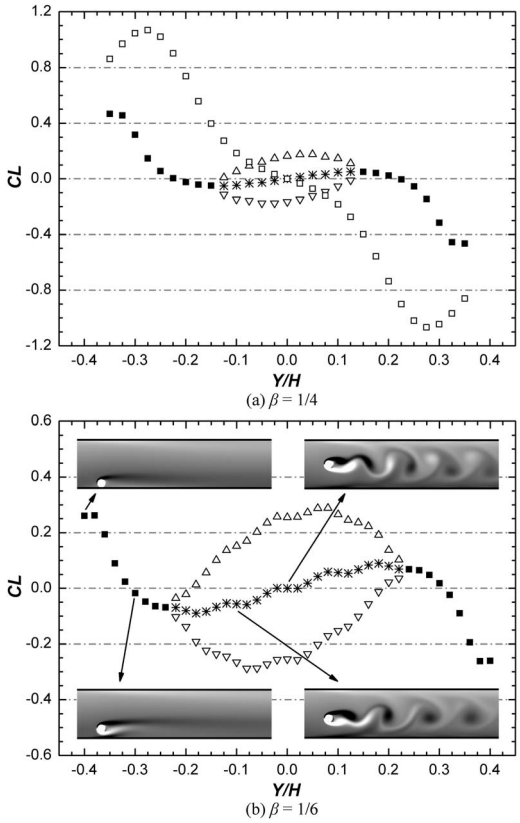

FIG. 20. Lift coefficient for flow past a stationary cylinder placed at different transverse positions in a parallel-wall channel at $\beta = 1/4$ and $\beta = 1/6$. The hollow squares represent the lift coefficients from the steady flow states for $Re = 20$ and $\beta = 1/4$. For $Re = 100$, $\beta = 1/4$, and $\beta = 1/6$, the solid squares represent the lift coefficients from the steady flow states, the upper and lower lows of triangles represent the maximum and minimum lift coefficients of the cylinder at the periodic flow states, respectively, and the stars represent the mean values of the maximum and minimum lift coefficients.

As shown in Fig. 19(d), $\Delta\theta$ of $S/D = 2$ is always obviously larger than that of $S/D = 1.5$ and for most cases of both $S/D = 1.5$ and $S/D = 2$, $\Delta\theta$ of $M = 1$ is larger than that of $M = 0.1$. For $S/D = 1.5$ and $M = 0.1$, $\Delta\theta$ decreases monotonously with decreasing β. While for the other cases, as β decreases, $\Delta\theta$ first decreases and then increases and the turning points for $S/D = 1.5$ and $M = 1$, $S/D = 2$ and $M = 1$ and $S/D = 2$ and $M = 0.1$ are $\beta = 1/7$, $\beta = 1/7$ and $\beta = 1/5$, respectively.

D. The mechanism of the cylinder oscillations

In the present simulations, several distinct oscillations of one and two tandem cylinders during a Poiseuille-type flow are observed. For each case of the PFIV model system with moderate Reynolds numbers, there exists a critical mass, below which large-amplitude cylinder oscillation could be produced. The critical mass ratio of the two-cylinder system in the strong coupling regime is much larger than that of a single one. For the case of two tandem cylinders with a small blockage ratio, the cylinder vibration is exclusive, and as the blockage ratio is decreased to a critical value, the cylinder oscillation becomes bistable.

To have a better understanding for the mechanism of the observed phenomena, the lift coefficient of a stationary cylinder placed at different transverse positions in a parallel-wall channel is measured at $\beta = 1/4$ and $\beta = 1/6$. Figure 20 shows the computed lift coefficient versus transverse position. As shown in Fig. 20(a), for $\beta = 1/4$ and $Re = 20$, the flow always behaves as a steady state as the cylinder is placed at any transverse position. There is only one steady equilibrium position at $Y/H = 0$ with a negative gradient of lift coefficient $\Gamma = \partial C_L/\partial Y$, which represents that as a cylinder is placed

close to the equilibrium position, there will be a hydrodynamic force pointing there. For the case of a moving cylinder, when the cylinder deviates from the equilibrium position, there will be a restoring force to pull the cylinder back to the equilibrium position, which brings about the rest regime for the low Reynolds number. For both $\beta = 1/4$ and $\beta = 1/6$ with $Re = 100$, results demonstrate that when the cylinder is placed near either channel wall, vortex shedding will be suppressed entirely (see the flow patterns at top-left and bottom-left of Fig. 20(b)) and the lift force is a constant number. As the gap between the cylinder and the channel wall G/D increases to a threshold, the flow translates to a periodic regime with a constant fluctuation of C_L and a single row of same-sign vortices appears gradually in the wake of the cylinder (see the flow pattern at bottom-right of Fig. 20(b)). When the cylinder is placed near the channel centerline, a wake structure with two rows of alternately rotating vortices is formed (see the flow pattern at up-right of Fig. 20(b)). Three equilibrium positions, at where the mean lift coefficient is zero, are observed. In the centerline of the channel, there is an unsteady equilibrium position with a positive Γ, representing that as a cylinder is placed close to the centerline, there is a mean lift force away from there. At each side of channel, there is a steady equilibrium position with a negative Γ, and the equilibrium positions are symmetrically positioned around the channel centerline. For the case of a freely moving cylinder, when a cylinder is close to an unsteady equilibrium position, there will be a hydrodynamic force to push the cylinder away from there, and when a cylinder deviates slightly from a steady equilibrium position, there will be a restoring force pulling the cylinder back there, as similar as a spring. For the case of an isolated cylinder with moderate Reynolds numbers, after a sufficiently long time, the cylinder will be captured by either steady equilibrium position. When the mass ratio of the cylinder is low, the motion of the cylinder is sensitive to the hydrodynamic force and a large-amplitude oscillation will be excited by the fluid-structure interaction and the cylinder oscillation becomes stronger and stronger with increasing Re due to the shedding vortices. The above discussion explains the observed biased non-periodic vibration for $M = 1$ and the biased periodic vibration with the vibration amplitude and frequency increases with increasing Re for $M = 0.1$, as shown in Fig. 7.

For the case of two-cylinder system with small spacing, the gap flow will have a complicated strong influence on each cylinder and both the cylinders will undergo oscillations with larger amplitudes than that of an isolated one. In the strong coupling regime, the behaviors of the gap flow and the cylinder motion are sensitive to the separation, which has also been observed of VIV of two elastically mounted cylinders.[10–13] As we have observed above, when the separation is changed between 1.25 and 3, the cylinder motions behave as a variety of distinct oscillation states due to the shedding vortices and the gap flow, and the critical mass ratio of two tandem cylinders with small spacing is much larger than that of a single one.

As shown in Fig. 20, for $\beta = 1/4$, the two steady equilibrium positions are of about $Y/H = -0.225$ and $Y/H = 0.225$, representing the distance between the two equilibrium positions is about $1.8D$. For $\beta = 1/6$, the two steady equilibrium positions are of about $Y/H = -0.31$ and $Y/H = 0.31$, representing the distance between the two equilibrium positions is about $3.7D$. In the vibration regime, the wake of the front oscillating cylinder will produce a zone of negative pressure. For a large blockage ratio, the channel is narrow and the distance between the two equilibrium positions is small, so the rear cylinder will be easily captured by the negative pressure zone behind the front cylinder and will oscillate together with the front cylinder at the same side of the channel, which brings about the oscillation Regime I. While for a small blockage ratio, the channel is wide and the distance between the two equilibrium positions is large, so in the vibration regime, besides the oscillation Regime I, another oscillation Regime II could also be excited. In Regime II, as the cylinders begin to oscillate, the two cylinders are separately captured by the two steady equilibrium positions. The distance between the two equilibrium positions is so large and the negative pressure zone behind the front cylinder is not strong enough to attract the rear cylinder to its wake, so the two cylinders will oscillate around their oscillation axes at different sides of the channel.

In Figs. 19(a) and 19(c) sometimes St_v decreases as A/D increases with decreasing β, which is different from that observed in Figs. 7, 15(a), and 15(c), at where St_v increases as A/D increases with increasing Re. Such a discrepancy is mainly produced by the fluid-structure interaction in combination with the wall confinement.

As a cylinder is close to either channel wall, the shear layer induced by the wall will have a repulsive force to the cylinder. In the vibration Regime I, the cylinders undergo stronger oscillations than that of a single cylinder because of the hydrodynamic force induced by the gap flow. For the case of a large blockage ratio, which represents a narrow channel, the strong cylinder oscillation in combination with the strong wall confinement will make the cylinders oscillate fast with small amplitudes between the two channel walls, as show in Figs. 19(a) and 19(c). As β is decreased, the wall confinement becomes weak, the vibration frequencies decrease and the oscillation amplitudes increase due to the increase of the distance between the two walls. When β is decreased to a threshold, the cylinders are mainly captured by one equilibrium position and the oscillations are not strong enough to close the wall at the opposite side of the channel, which induces the biased vibration, and the biased degrees of both cylinders increase with decreasing β, see Fig. 19(b).

Based on the above discussion, the complicated change of the oscillation amplitude observed in Figs. 19(a) and 19(c) is induced by the complicated effects of the fluid-oscillator interaction and the wall confinement.

V. CONCLUSION

Flow-induced vibrations of one and two tandem circular cylinders in a parallel-wall channel are simulated by using the lattice Boltzmann method. The cylinders are fixed in the streamwise direction, while are free to move in the cross-flow direction. The effects of Reynolds number, streamwise separation, mass ratio, and blockage ratio on the motions of cylinders and fluids are investigated, respectively. The main conclusions can be drawn as follows:

(1) For the case of an isolated cylinder, as the Reynolds number is changed, no large-amplitude oscillation can be excited at a moderate mass ratio. While for a low mass ratio, as the Reynolds number is increased to a threshold, a biased periodic vibration with a considerable amplitude is observed. For the case of two tandem cylinders, two distinct steady regimes: the symmetrical steady and biased steady regimes, and several oscillation regimes, e.g., the symmetrical periodic vibration, biased periodic vibration, quasi-periodic vibration and period-doubling vibration regimes with the corresponding flow structures are observed.
(2) The phenomenon of critical mass ratio exists extensively in PFIV and the critical mass ratio of two tandem cylinders in the strong coupling regime is about an order of magnitude larger than that of an isolated cylinder. The mechanism of the phenomenon is that the gap flow between the two cylinders will have a strong effect on each cylinder.
(3) There is a critical blockage ratio, below which the vibration type of the cylinders is exclusive, while beyond which the cylinder oscillation is bistable. The appearance of the vibration Regime II is found mainly dependent on the blockage ratio, while not the mass ratio and the streamwise separation.
(4) By an analysis of the lift distribution of a stationary cylinder placed at different transverse positions of a plane channel, several steady and unsteady equilibrium positions are observed based on gradient of lift coefficient near the equilibrium positions. The cylinder oscillation is mainly excited by the complicated influence of the gradient of lift coefficient near the equilibrium positions, the shedding vortices, the wall confinement and the gap flow. The bistable oscillation regime observed at low blockage ratios is mainly produced by the large distance between the two steady equilibrium positions, at where the rear cylinder cannot be attracted to the wake of the front one with a negative pressure and the two cylinders oscillate apart from each other at different sides of the channel.

ACKNOWLEDGMENTS

The authors acknowledge financial support from the Major Program of National Natural Science Foundation of China (Grant No. 11132008).

[1] C. H. K. Williamson and R. Govardhan, "Vortex-induced vibrations," Ann. Rev. Fluid Mech. **36**, 413 (2004).
[2] D. Brika and A. Laneville, "Vortex-induced vibrations of a long flexible circular cylinder," J. Fluid Mech. **250**, 481 (1993).
[3] C. C. Feng, "The measurements of vortex-induced effects in flow past a stationary and oscillating circular and D-section cylinders," Master's thesis, Univ. BC, Vancouver, Canada, 1968.
[4] C. Y. Zhou, R. M. C. So, and K. Lam "Vortex-induced vibrations of an elastic circular cylinder,"J. Fluids Struct. **13**, 165 (1999).
[5] R. Govardhan and C. H. K. Williamson, "Modes of vortex formation and frequency response of a freely vibrating cylinder," J. Fluid Mech. **420**, 85 (2000).
[6] R. Govardhan and C. H. K. Williamson, "Resonance forever: existence of a critical mass and an infinite regime of resonance in vortex-induced vibration," J. Fluid Mech. **473**, 147 (2002).
[7] N. Jauvtis and C. H. K. Williamson, "Vortex-induced vibration of a cylinder with two degrees of freedom," J. Fluids Struct. **17**, 1035 (2003).
[8] S. Mittal and S. Singh, "Vortex-induced vibrations at subcritical Re," J. Fluid Mech. **534**, 185 (2005).
[9] T. K. Prasanth, S. Behara, S. P. Singh, R. Kumar, and S. Mittal, "Effect of blockage on vortex-induced vibrations at low Reynolds numbers," J. Fluids Struct. **22**, 865 (2006).
[10] M. M. Zdravkovich, "Flow-induced oscillations of two interfering circular cylinders," J. Sound Vib. **101**, 511 (1985).
[11] G. V. Papaioannou, D. K. P. Yue, M. S. Triantafyllou, and G. E. Karniadakis, "On the effect of spacing on the vortex-induced vibrations of two tandem cylinders," J. Fluids Struct. **24**, 833 (2008).
[12] T. K. Prasanth and S. Mittal, "Flow-induced oscillation of two circular cylinders in tandem arrangement at low Re," J. Fluids Struct. **25**, 1029 (2009).
[13] I. Borazjani and F. Sotiropoulos, "Vortex-induced vibrations of two cylinders in tandem arrangement in the proximity-wake interference region," J. Fluid Mech. **621**, 321 (2009).
[14] K. Ryan, C. J. Pregnalato, M. C. Thompson, and K. Hourigan, "Flow-induced vibrations of a tethered circular cylinder," J. Fluids Struct. **19**, 1085 (2004).
[15] J. Carberry and J. Sheridan, "Wake states of a tethered cylinder," J. Fluid Mech. **592**, 1 (2007).
[16] R. Govardhan and C. H. K. Williamson, "Vortex-induced vibrations of a sphere," J. Fluid Mech. **531**, 11 (2005).
[17] R. van Hout, A. Krakovich, and O. Gottlieb, "Time resolved measurements of vortex-induced vibrations of a tethered sphere in uniform flow," Phys. Fluids **22**, 087101 (2010).
[18] R. Jiang, J. Lin, and Z. Chen, "Vibrations of cylindrical objects obstructing a Poiseuille-type flow," Phys. Rev. E **88**, 023009 (2013).
[19] J. Lin, R. Jiang, Z. Chen, and X. Ku, "Poiseuille flow-induced vibrations of two cylinders in tandem," J. Fluids Struct. **40**, 70 (2013).
[20] P. W. Bearman and M. M. Zdravkovich, "Flow around a circular cylinder near a plane boundary," J. Fluid Mech. **89**, 33 (1978).
[21] L. Zovatto and G. Pedrizzetti, "Flow about a circular cylinder between parallel walls," J. Fluid Mech. **440**, 1 (2001).
[22] N. Kanaris, D. Grigoriadis, and S. Kassinos, "Three dimensional flow around a circular cylinder confined in a plane channel," Phys. Fluids **23**, 064106 (2011).
[23] S. Succi, *The Lattice Boltzmann Method for Fluid Dynamics and Beyond* (Oxford University Press, 2001).
[24] P. L. Bhatnagar, E. P. Gross, and M. Krook, "A model for collision processes in gases. I. Small amplitude processes in charged and neutral one-component systems," Phys. Rev. **94**, 511 (1954).
[25] H. Chen, S. Chen, and W. H. Matthaeus, "Recovery of the Navier-Stokes equation using a lattice-gas Boltzmann method," Phys. Rev. A **45**, R5339 (1992).
[26] Y. H. Qian, D. d'Humières, and P. Lallemand, Lattice BGK models for Navier-Stokes equation," Europhys. Lett. **17**, 479 (1992).
[27] X. Y. He and L. S. Luo, "Lattice Boltzmann model for the incompressible Navier-Stokes equation," J. Stat. Phys. **88**, 927 (1997).
[28] A. J. C. Ladd, "Numerical simulations of particulate suspensions via a discretized Boltzmann equation. Part 1. Theoretical foundation," J. Fluid Mech. **271**, 285 (1994).
[29] R. W. Mei, L. S. Luo, and W. Shyy, "An accurate curved boundary treatment in the lattice Boltzmann method," J. Comput. Phys. **155**, 307 (1999).
[30] Z. Guo, C. Zheng, and B. Shi, "An extrapolation method for boundary conditions in lattice Boltzmann method," Phys. Fluids **14**, 2007 (2002).
[31] M. P. Allen and D. J. Tildesley, *Computer Simulation of Liquid* (Clarendon Oxford, 1987).
[32] H. T. Ahn and Y. Kallinderis, "Strongly coupled flow/structure interactions with a geometrically conservative ALE scheme on general hybrid meshes," J. Comput. Phys. **219**, 671 (2006).